Underwater Spontaneous Pumpless Transportation of Nonpolar Organic Liquids on Extreme Wettability Patterns

Shuai Huang[1], Jinlong Song[1], Yao Lu[2], Faze Chen[1], Huanxi Zheng[1], Xiaolong Yang[1], Xin Liu[1], Jing Sun[1], Claire J. Carmalt[2], Ivan P. Parkin[2], Wenji Xu[1]*

1 Key Laboratory for Precision and Non-Traditional Machining Technology of Ministry of Education, Dalian University of Technology, Dalian 116024, China

2 Materials Chemistry Research Centre, Department of Chemistry, University College London, 20 Gordon Street, London, WC1H 0AJ, UK

KEYWORDS: underwater spontaneous pumpless transportation, extreme wettability patterns, nonpolar organic liquids, cold plasma, superoleophobic surface

ABSTRACT: Spontaneous pumpless transportation (SPT) of liquids has generated tremendous demands in microfluidic systems and advanced devices. However, the transportation of nonpolar organic liquids on open platforms underwater remains a challenge because most existing SPT systems are only designed for use in air. Here, we report a surface-tension-driven SPT system to transport various nonpolar organic liquids using underwater extreme wettability patterns. The

patterns were fabricated with a wedge-shaped superoleophilic track on a superoleophobic background by combining $CuCl_2$ etching, stearic acid modification and mask-based nitrogen cold plasma treatment. Three types of underwater SPT processes, horizontal transport, tilted transport, and directional transport, were studied experimentally and theoretically. For horizontal SPT and tilted SPT, the capillary force was the main driving force, which depended on the wedge angle of the superoleophilic track. The excellent transportation ability of horizontal SPT of underwater liquid droplets was obtained at a wedge angle of 3°-5°. The maximum moving height of organic liquids on the tilted SPT transport was obtained at an angle of 8°. For directional SPT, organic liquids did not drop off in the moving process because of the constraint imposed by surface tension, resulting in the sustained directional transport with long distances and complex trajectories.

1. Introduction

Roots of trees can absorb and transport water from the soil up to the crowns. This quite pervasive natural phenomenon generates research interest into the spontaneous pumpless transport (SPT) of fluid. This has become increasingly popular for energy-saving and micro-/nano- fluid analysis systems, especially for microfluidic chips, biomedical testing, micro-pumps and other energy fields.[1-5] To date, there are only a few methods to achieve SPT of fluids, such as using wettability gradient [6, 7], using special geometrical shape [8-10], using external stimuli induced wettability change [11, 12], and using extreme wettability patterns [13, 14]. For example, Chaudhury *et al*. [6] used decyltrichlorosilane modification to obtain a wettability gradient region on silicon wafer and further realized the SPT of water on that region with an average velocity of 1 to 2 mm/s; Quere *et al*. [8] used a conical fibre to realize the SPT of water by relying on the

different Laplace pressure of region with different radius; Khare *et al*. [11] relied on electrowetting phenomenon and exerted different voltage on different region to realize the voltage stimuli induced wettability change and the SPT of water; Megaridis *et al*. [13] employed the extreme wettability patterns, which contain both super-phobic area and super-philic area on the same surface, to realize the SPT of water with a flow rate of up to 300 mm/s; Tseng *et al*. [14-17] conducted the experiments for water droplets on extreme wettability patterns with a maximum speed of 420 mm/s, and applied this technique to microfluidic systems. Compared with other methods, extreme wettability patterns have more advantage in the SPT because of relatively high transport speed. Although some investigations on the SPT of liquid have been conducted, the existing work are invariably limited to processes in air. Underwater SPT of organic liquids, which has potentially extensive applications in underwater fluid delivery systems, micro detectors and underwater intelligent systems, has not been achieved. Similar in air, underwater extreme wettability patterns maybe realize the underwater SPT of organic liquids with high transport speed. For in air, the main driving force of using extreme wettability patterns is capillary force. However, the underwater environment is really different with the environment in air. The buoyancy maybe make an influence on the underwater SPT of organic liquids. All these possibility need to be studied. In addition, the fabrication method of the underwater extreme wettability patterns still have not been reported, because the wettability behaves completely differently underwater from air phases, which brings a new challenge to realize the underwater SPT of organic liquids with high transport speed by using underwater extreme wettability patterns.

Here, we realized the underwater spontaneous pumpless horizontal transport (SPHT), spontaneous pumpless tilted transport (SPTT) and spontaneous pumpless directional transport

(SPDT) of organic liquids on underwater extreme wettability patterns with superoleophilic track and superoleophobic backgrounds. These surface were fabricated successfully by $CuCl_2$ etching, stearic acid modification and nitrogen cold plasma treatment with masks on aluminum substrates. The excellent SPHT of underwater liquid droplets was obtained at wedge angles of 3°-5°. The maximum height of underwater SPTT of different organic liquids is directly proportional to the initial velocity. The moving distances and trajectories of SPDT were found to be based on the surface tension of the organic liquid.

2. Results and discussion

2.1 Preparation of underwater extreme wettability patterns

The fabrication processes to make underwater extreme wettability patterns are shown in Fig.1. After removal of the oxide layer, the aluminum plate was immersed in the 1 mol/L aqueous $CuCl_2$ solution for 20 s to fabricate the micro-/nano-structures[18]. The etched aluminum plate was then immersed in the 0.05 mol/L ethanol solution of stearic acid for approximately 20 min to reduce the surface energy. After the aforementioned two steps, a superhydrophobic surface was obtained. Then, an atmospheric cold plasma jet with mask was used to prepare patterns with different wettability[19]. Since only the area touched with the plasma jet became superhydrophilic, the shape of the patterns on the mask decided the shape of the extreme wettability patterns. Five nonpolar organic liquids (paraffin oil, hexane, peanut oil, dichloromethane and diesel oil) with different density, surface tension and kinematic viscosity were used in this study and dyed for visualization (Table S1, Supporting Information). The volume of the liquid droplet in the study was ~4.4 μL based on our devices (handling capability of droplet volume is not less than 250μL). The surface morphology and chemical composition of the Al surfaces were characterized by scanning electron microscopy (SEM, SUPRA 55 SAPPHIRE, Germany),

energy-dispersive X-ray spectroscope (EDS, SUPRA 55 SAPPHIRE, Germany) and Fourier transform infrared spectroscopy (FTIR, JACSCO, Japan).

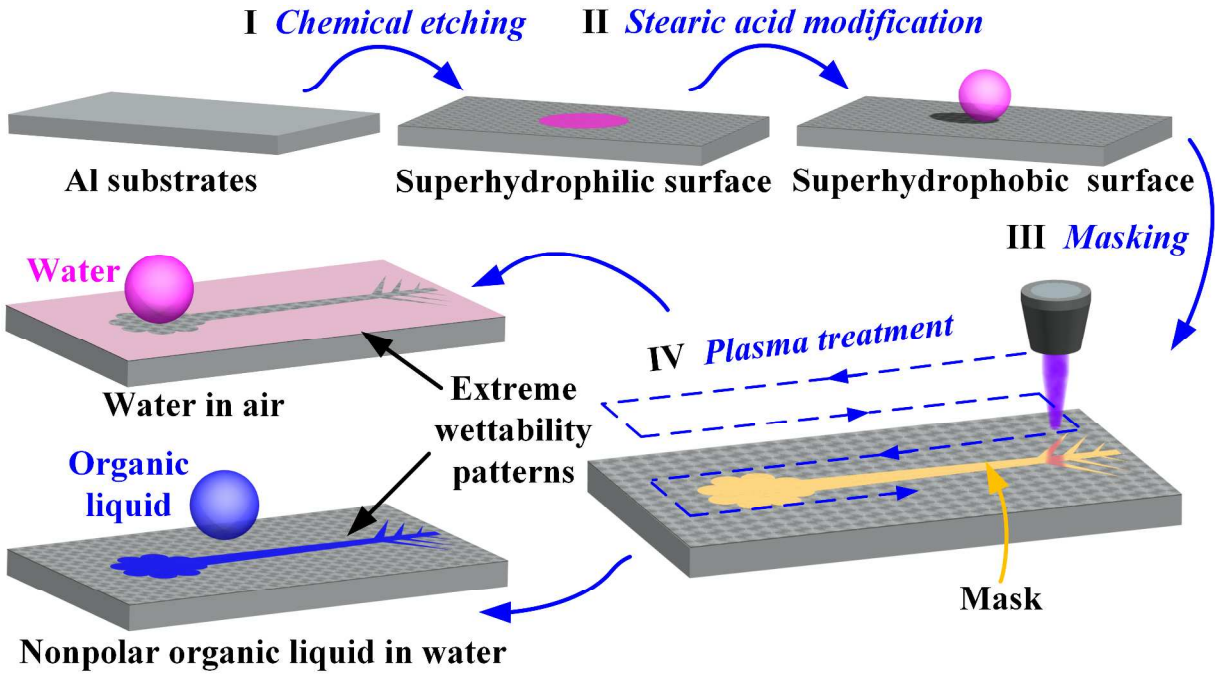

Figure 1. Fabrication processes of the underwater extreme wettability patterns. Step I: Chemical-etching process was used to fabricate a superhydrophilic surface. Step II: Surface energy was reduced by stearic acid. Step III: The superhydrophobic surface was masked in the desired pattern. Step IV: Atmospheric cold plasma jet treatment was applied with mask to prepare patterns with different wettability.

2.2 Underwater extreme wettability patterns

After $CuCl_2$ etching and stearic acid modification, the Al surfaces were superhydrophobic with a water contact angle of 158° and a sliding angle of only 1°, as shown in Figure 2(a). The superhydrophobic properties were the result of the irregular micro/nano-rectangular pits and protrusion structures obtained from etching [Fig.2 (a1)] and the low surface energy due to stearic acid modification. The peaks due to C, N, O in the EDS spectrum and the vibration peaks of -

CH_2-, -CH_3 groups in the FTIR spectrum were all from stearic acid, which was coordinated to the Al surfaces.[20-22] This superhydrophobic Al surface could be effectively transformed into a superhydrophilic surface after treatment with an atmospheric cold plasma.[23] The treatment process of the plasma is shown in Figure 2 (b). Water droplets spread quickly on the plasma-treated surface [Fig. 2 (c)]. The transition of the wettability after plasma treatment was not due to a change in surface morphology but was the result of removal of the low surface energy groups (-CH_2-, -CH_3). Figures 2(c1) - 2(c3) are the SEM images, EDS and FTIR spectrum of the superhydrophilic Al surfaces after the cold plasma treatment, respectively. The morphology of the Al surfaces after the cold plasma treatment was found to be similar to the superhydrophobic surface and still consisted of micro/nano-structures of irregularly rectangular pits and protrusions. However, the results of EDS showed that the amount of C reduced from 2.89 wt% to 1.68 wt% after plasma treatment, which is a decline of approximately 41.87%. Similarly, the content of oxygen also reduced from 1.30 wt% to 1.11 wt%. In addition, the characteristic peaks from -CH_2-, -CH_3 groups in FTIR spectrum at 2960 cm^{-1}, 2919 cm^{-1} and 2852 cm^{-1} showed significantly reduced intensity. This is the results of the active particles in the cold plasma (Section S1, Supporting Information) potentially minimizing the stearic acid and reducing the number of groups of -CH_2-, -CH_3, C=O and Al-O on the surface. The superhydrophobic-superhydrophilic wettability patterns in air can be fabricated by combining the cold plasma treatment and a mask with a desired shape of the patterns, as shown in Figure 2(d). When the superhydrophobic-superhydrophilic wettability patterns were immersed in water, air was trapped in the micro/nanostructures in the superhydrophobic region and was easily displaced by organic liquids, resulting in underwater super-philic to nonpolar organic liquids with oil contact angle of 0° (this state was also defined as underwater superoleophilic) [24]. Conversely, for the

superhydrophilic region, the water penetrated and became entrapped between in the rough micro/nanostructures, forming a repellent conformal barrier to organic liquids because of the different polarity and underwater super-phobic to nonpolar organic liquids resulted (this state was also defined as underwater superoleophobic, as shown in Fig. S2, Fig. S3, Video S1 and Video S2, Supporting Information).

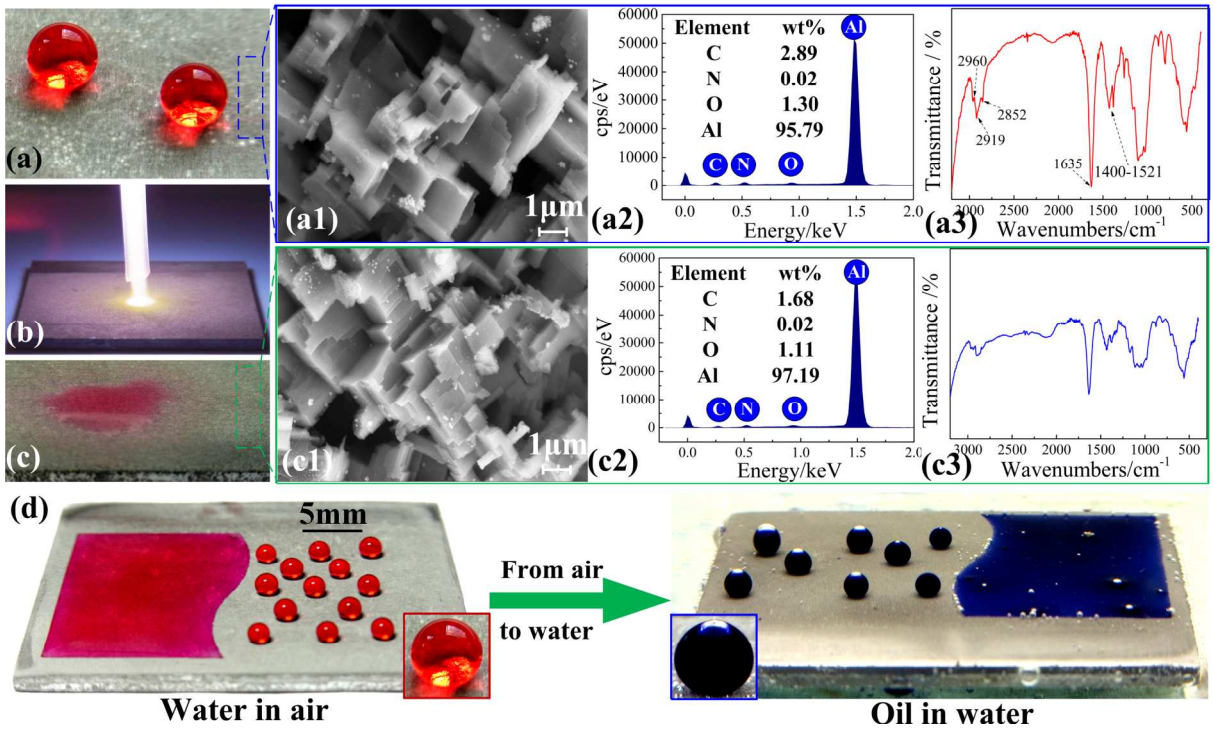

Figure 2. Characterizations of the extreme wettability patterns. (a) Images of superhydrophobic Al surface. (a1-a3) SEM images, EDS, FTIR of superhydrophobic Al surface, respectively. (b) The treatment processes of superhydrophobic Al surface by nitrogen cold plasma jet. (c) Images of superhydrophilic Al surface. (c1-c3) SEM images, EDS and FTIR spectrum of superhydrophilic Al surface, respectively. (d) Extreme wettability patterns (upper surface on Al substrates) of water in air (left) and dichloromethane in water (right).

Thus, the underwater superoleophobic-superoleophilic wettability patterns for organic liquids, e.g. paraffin oil, hexane, peanut oil, dichloromethane and diesel oil, were eventually obtained, as

shown in Fig. 3. The underwater superoleophilic dot with a diameter of 0.5 mm was designed at the bottom [Fig. 3(a)] to stick the organic liquids with a density less than water. When the density was less than water (1, paraffin oil; 2, hexane; 3, peanut oil; 5, diesel oil.), the buoyancy effect was dominant, and the droplets were stretched, as shown in Fig. 3(c). In comparison, the liquid droplet (4, dichloromethane) was approximately spherical as its density was greater than that of water.

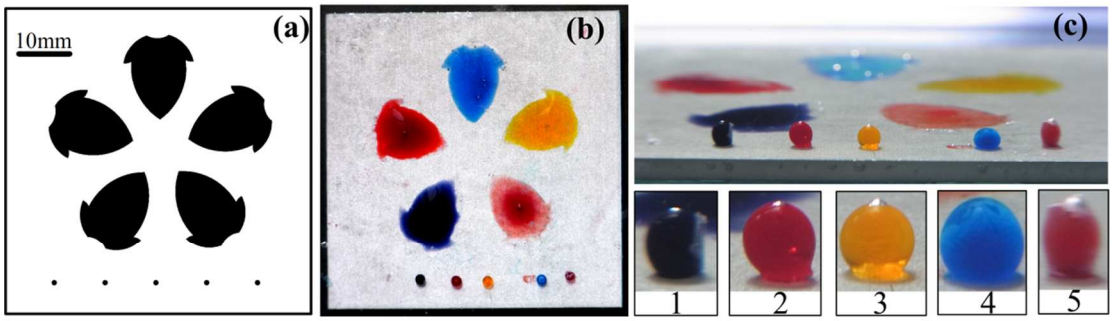

Figure 3. (a) Masking template for (b and c) organic liquids on underwater extreme wettability patterns. (b) Top view and (c) side view of organic liquids (5 μL) on underwater extreme wettability patterns: 1, paraffin oil; 2, hexane; 3, peanut oil; 4, dichloromethane; 5, diesel oil.

2.3 Underwater spontaneous pumpless horizontal transport

Based on the aforementioned method, the underwater extreme wettability patterns with wedge-shaped superoleophilic tracks and superoleophobic backgrounds were fabricated to study the surface-tension-driven underwater spontaneous pumpless horizontal transport (SPHT) of nonpolar organic liquids. On the pre-suffused superoleophilic track, a single liquid droplet evolved from a spherical liquid droplet into either a fast-moving liquid front or slow-moving liquid bulge, which continuously extended to the superoleophilic track, and kept shrinking until disappearing, as shown in Fig. 4(a) (Video S3, Supporting Information). The liquid front moved

faster than the bulge because the liquid front was not only driven by hemi-wicking through the micro/nano-scale roughness features but driven by surface tension, while the bulge was only driven by the surface tension through the wedge angle structure. With the weakening of the capillary force, the difference of force between liquid front and liquid bulge was also weakened, and finally the liquid front and liquid bulge tended to merge. The organic liquid could not achieve smooth transportation without pre-suffused during the experimental process, because the interface between water and the superhydrophobic track was filled with air before pre-suffused and the air would therefore obstruct the transport process.

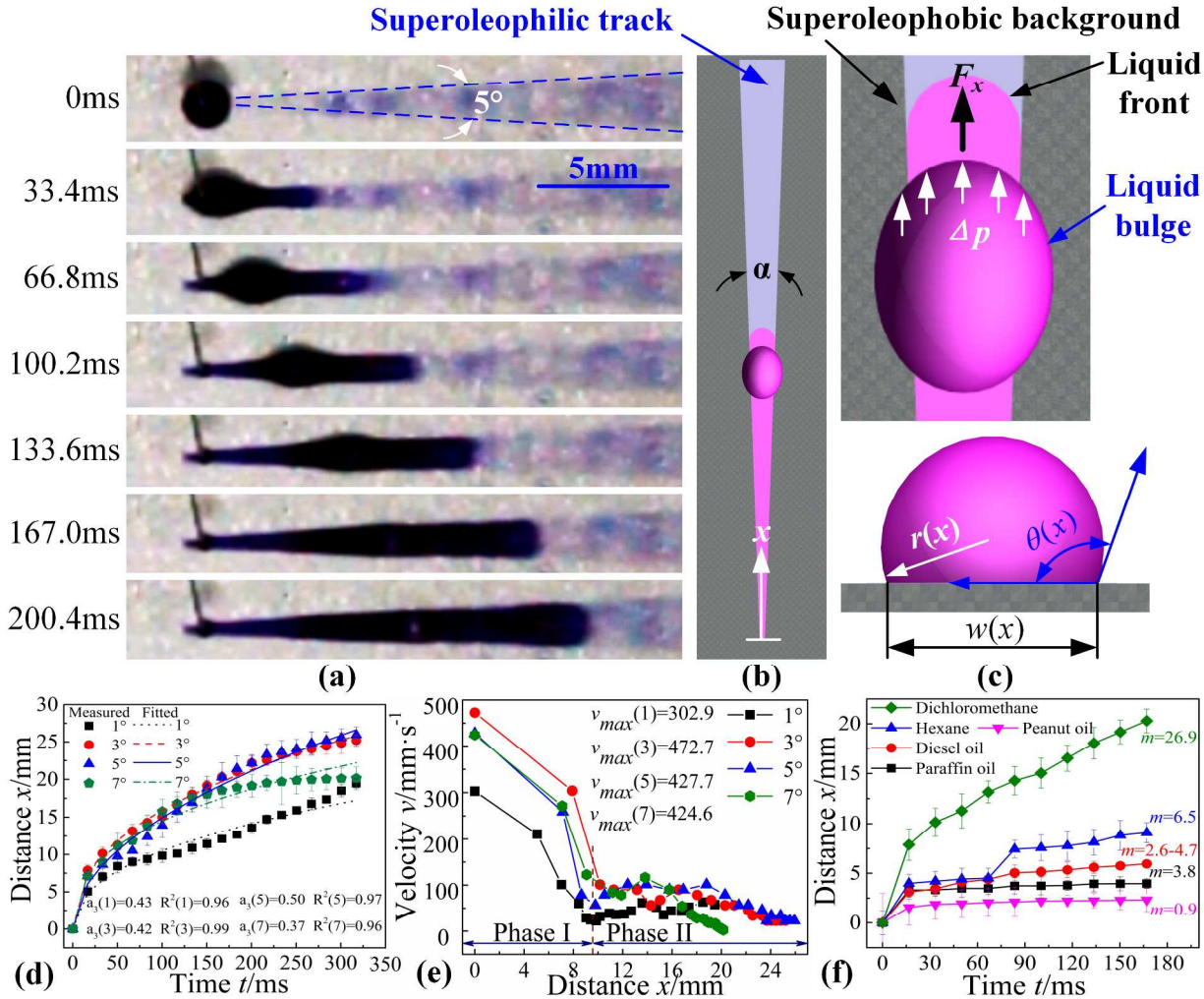

Figure 4. (a) Time-lapse photography (top view) of dichloromethane droplets transport on the horizontal extreme wettability patterns. (b) Schematic of transportation process of organic liquids

droplets (α is the wedge angle, °). (c) Schematic of the organic liquids droplets spontaneously driven by the surface tension. (d) Variation in the moving distances of the liquid front with time ($a_i(j)$ is the fitting coefficients; $R^2(i)$ is the is the significance level). (e) Velocity as a function of the distance along the track (v_{max} is the maximum velocity, mm/s). (f) Variation in the moving distances with time at a wedge angle of 4° for different organic liquids.

During the process of SPHT, as shown in Figs. 4(b) and 4(c), the Laplace pressure difference of organic liquids droplets in x direction, ΔP, can be estimated as follows[13]:

$$\Delta p \sim \frac{\gamma_{OW}}{r(x)} \approx 4\gamma_{OW} \frac{\sin[\theta(x)]}{a + 2x\tan\frac{\alpha}{2}} \qquad (1)$$

where, γ_{ow} is the surface energy per unit interface area between organic liquids and water, $r(x)$ is the local curvature of the liquid on the superoleophilic track [$r(x) = w(x)/2\sin\theta(x)$][13]; $\theta(x)$ is the contact angle of the organic liquid droplet; a is initial width (where $x = 0$) of the superoleophilic track; α is the wedge angle. The force of the organic liquid droplet in x direction F_x can be expressed as follows: $F_x = \Delta P \cdot S(x)$. Where $S(x)$ denotes the cross section area in x the direction, which is proportional to $\pi r^2(x)/2$, as the rivulet of liquid accumulating on wedge track is semi-conical [13], F_x can therefore be estimated by the following equation:

$$F_x = \Delta P \cdot S(x) \sim \pi\gamma_{OW} \frac{a + 2x\tan\frac{\alpha}{2}}{4\sin[\theta(x)]} \qquad (2)$$

The contact angle $\theta(x)$ is a function of the position x along the superoleophilic track. Brinkmann *et al* [25] analyzed wetting morphologies of water in air on the superoleophilic track without wedge angle by using numerical simulation. However, the complex laws of $\theta(x)$ corresponding to the movement of underwater liquid along the wedge angle still need further

investigation. Thus, it is relatively difficult to calculate the magnitude of F_x using Eq. (2). Therefore, the relationship between the displacement and time at different wedge angles in the underwater SPHT of organic liquids droplet was calculated by an experimental method to further study the dynamic characteristics including velocity and acceleration. Dichloromethane was used as typical non-polar organic liquid to find out which wedge angle could obtain optimized SPHT.

All the moving distances of underwater dichloromethane droplets on different wedge-angles superoleophilic tracks increased gradually over time, as shown in Fig.4(d). The Washburn equation[26-28] describes the dynamics of capillary flow. In case of a fully wettable capillary, variation of the liquid moving distances x with time t can be described as follows:

$$x^2 = (\gamma D/4\eta)\,t \qquad (3)$$

Where γ, η and D are all constants that represent the liquid surface tension, the liquid dynamic viscosity, and the pore diameter of the plate surface, respectively. As shown in Eq. (3), it cannot reflect our focus which is the relationship of the dynamics with different wedge angles α. Therefore, according to the style of the Washburn equation, the relationship among the moving distance of liquid droplet, wedge angle α and time t was assumed as follows:

$$x(\alpha,t) = \sqrt{\gamma D/4\eta}\;\alpha^{a_1}\,t^{a_2} \qquad (4)$$

where, a_1, a_2 are all constants. Taking logarithms of both sides of Eq. (4), and making linear regression on the experimental values in Fig.4(d), the following equations are valid: $x(\alpha,t) = 1.556\alpha^{0.174}t^{0.430}$, $R^2 = 0.901$. The Washburn equation (3) shows that the wetting morphologies should correspond with $x \sim t^{1/2}$, but the characteristic $t^{0.43}$ in this study was slightly less than $t^{1/2}$. While at $\alpha = 5°$, we can obtain $a_3 = 0.50$ and $R^2 = 0.97$, which was completely

consistent with the Washburn equation. The exponent deviations may be caused by the factor of α and the different working environment.

All the velocities of the underwater dichloromethane droplet at different wedge angles decreased sharply at first and then kept stable. The maximum initial velocity of 472.7 mm/s was obtained at a 3° wedge angle, as shown in Fig.4 (e). Meanwhile, the average velocities with wedge angles of 3° and 5° were almost equal, and both larger than those with wedge angles of 1° and 7° [Fig.4 (d)]. When the width $w(x)$ of the superoleophilic track was less than the capillary length $k^{-1} = \sqrt{\gamma / \rho g}$ (k^{-1}, γ, ρ, and g are the capillary length, surface tension, density and acceleration due to gravity, respectively), capillarity was evident, and the velocity was relatively higher [phase I of Fig.4(e)]. While for $w(x) > k^{-1}$, the capillarity was not apparent, and the velocity was comparatively lower [phase II of Fig.4(e)]. When $\alpha = 5°$, the value of k^{-1} can be calculated ($k^{-1} = 1.3$mm), and then the value of $x = 9.6$mm, which is how the dividing line of phase I and phase II in Fig.4(e), was calculated.

The acceleration of the motion of underwater dichloromethane droplet was obtained by using second order difference on $x = x(t)$. When the wedge angles were 1°, 3°, 5° and 7°, the corresponding initial accelerations were 6.0 m/s^2, 11.1 m/s^2, 10.45 m/s^2 and 9.17 m/s^2, respectively. Thus, the corresponding initial forces [$F(x = 0)$] were 35.2 μN, 64.7 μN, 60.8 μN, 53.3 μN, respectively (the mass of the dichloromethane droplet was about 5.82 mg). The average velocity and initial accelerations at 3° and 5° were larger than that at 1° and 7°, indicating better transport ability. Thus, the excellent SPHT of underwater organic liquids was obtained at wedge angles of 3°-5°.

The transport ability of the underwater SPHT was also affected by the surface tension and kinematic viscosity of organic liquids. Fig. 4(f) shows the variation in the moving distances with time at a wedge angle of 4° for different organic liquids. Experimental results shown that the higher $\sqrt{\gamma/\eta}$ enabled the greater liquid travel, which was also correspond with the Eq. (3). In Fig. 4(f), $m = \sqrt{\gamma/\eta}$, and η denotes the kinematic viscosity of liquid.

The aforementioned dynamic analysis of organic liquids in the underwater transport process on the horizontal extreme wettability patterns indicate that SPHT of underwater organic liquids can be achieved on the underwater extreme wettability patterns with wedge angles.

2.4 Underwater spontaneous pumpless tilted transport

The feasibility of underwater SPT of organic liquid droplets using the underwater extreme wettability patterns with wedge-shaped tracks and superoleophobic backgrounds was verified by the aforementioned study. However, the narrow width of the superoleophilic track meant that the liquid droplets could not easily be initially dropped on the track. In order to reduce the difficulty in operation of liquid droplets, root-like patterns were designed, as shown in Fig.5 (a). The underwater liquid droplets on any area around the root-like patterns, including the superoleophilic track and superoleophobic background, were sucked by the 'root-like' parts and transported to the 'trunk-like' section, and then to the 'crown', as shown in Figs. 5(b)-5(d). This idea was inspired by natural phenomena, such as water being absorbed by roots from the soil and being transported to the crowns of trees. After 70 liquid drops, approximately 307.3 μL of dichloromethane was successfully transported to the reservoir while only two drops with smaller diameters remained in the root region (Video S4, Supporting Information).

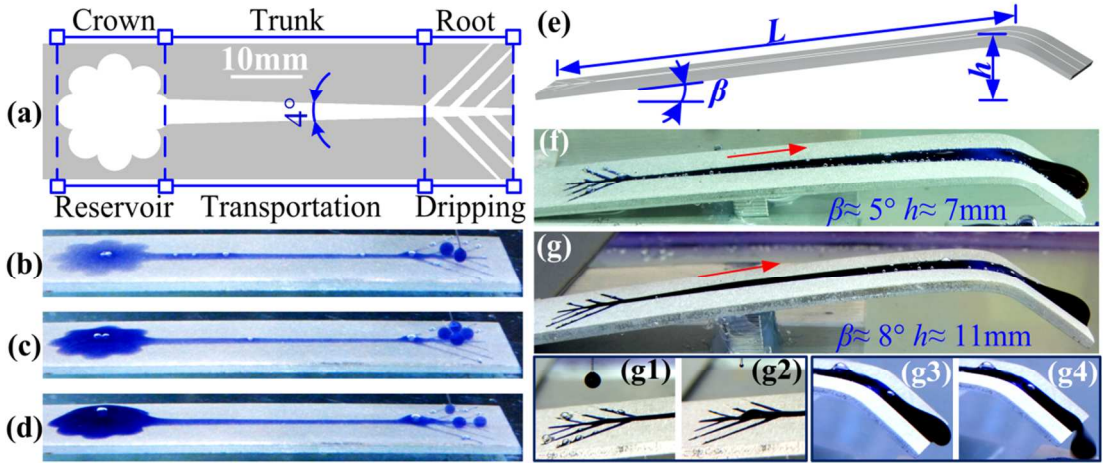

Figure 5. (a) Schematic of the root-like extreme wettability patterns. (b-d) Snapshots of dichloromethane (dyed for better visualization) after 10 drops (43.9 μL), 30 drops (131.7 μL) and 70 drops (307.3 μL), respectively. (e) Schematic of the root-like extreme wettability patterns for underwater spontaneous dichloromethane uphill transport (β is the tilted angle and the wedge-shaped angle of the superoleophilic track is 4°, L=80 mm). (f), (g) Images of the spontaneous dichloromethane transport with the tilted angle of 5°and 8°, respectively. (g1), (g2) The sucking and (g3), (g4) dropping processes of root-like extreme wettability patterns.

The underwater spontaneous pumpless tilted transport (SPTT) can be divided into two types: (1) anti-gravity pumpless uphill transport for heavy organic liquids which have a heavier density than water; (2) anti-buoyancy downhill pumpless transport for light organic liquids which have a lighter density than water. In order to obtain the Equation describing the maximum transport with uphill or downhill height, a series of theoretical and experimental analysis were done with the help of the root-like patterns, as shown in Fig.5 (e). Dichloromethane was used as typical heavy organic liquid to verify the consistency of theoretical and experimental results. The forces F_x of organic liquids along superoleophilic track can be estimated as:

$$F_x - [m(x)\mathrm{g} - \rho_{\mathrm{water}} g V(x)]\sin\beta = m(x)a(x) \qquad (5)$$

where, $m(x)$, $V(x)$ and $a(x)$ indicate the liquid mass, volume and acceleration at different positions, respectively. Brinkmann' research may be a valid reference to calculate the volume $V(x)$ [29]. Sustainable transport of organic liquids was conducted after the superoleophilic track was wetted. The transport process obeys the law of conservation of energy:

$$\frac{1}{2}mv_0^2 = \Delta E_{SE} + \mathrm{mg}\Delta h + \frac{1}{2}mv_x^2 + \Delta W \qquad (6)$$

where, v_0 is the initial velocity of liquid droplets; ΔE_{SE} is the variation in the surface energy of the liquid during transport; Δh denotes the vertical rise height of the liquid; v_x is the velocity of the liquid droplets on the underwater extreme wettability patterns; and ΔW denotes the work of extra forces (such as buoyancy, friction, etc.).

According to Eq. (6), the maximum underwater transport height $h_{\max}$ (when v_x=0) of organic liquids on the underwater extreme wettability patterns was thereby calculated as

$$h = v_0^2 / 2g - (\Delta E_{SE} + \Delta W) / mg \qquad (7)$$

For dichloromethane with v_0 of 461 mm/s, $h_{\max} = [10.8 - (\Delta E_{SE} + \Delta W) / mg]\mathrm{mm}$. Assuming the released surface energy of dichloromethane equilibrates the energy consumption of extra resistance (*e. g.*, hysteresis force, viscous force and friction force), thus the theoretical height $h_{\max}$ is about 10.8 mm. In the experiments, we found that for a tilted angle of 5°, 150 oil droplets (~658.5 μL) were elevated to the top of the underwater extreme wettability patterns within 450 s, with the height of SPTT being approximately 7 mm, as shown in Figure 5(f). For a tilted angle of 8°, dichloromethane droplets were continuously and spontaneously transported to an altitude of 11 mm with a flow rate of 1.14 μL/s, as shown in Fig.5 (g) and Video S5 in Supporting Information. However, for a tilted angle of 10°, the driving force was less than the resistance,

resulting in the liquid droplets remaining at the root of the underwater extreme wettability patterns and they could not be transported to the top (Fig. S4, Supporting Information). Thus, the experimental maximum transportation height of liquid droplets is approximately 11 mm, which is consistent with the theoretical value. Figs 5(g1)-5(g4) displays the processes of organic liquid droplets sucked by the roots and falling down at the terminal of the superoleophilic track (Video S6, Supporting Information).

2.5 Underwater spontaneous pumpless directional transport

The aforementioned parts discussed the surface-tension-driven underwater spontaneous horizontal-transport and anti-gravity or anti-buoyancy titled transport. In this part, we found that surface-tension-assisted gravity driven (gravity is the main driving force and the surface tension constrains the trajectory) and buoyancy driven underwater spontaneous pumpless directional transport (SPDT) could be realized on the extreme wettability patterns with the wedge-shaped tracks, as shown in Fig. S5(e) and 6(a), respectively. Heavy organic liquids (dichloromethane) moved downhill while light organic liquids (hexane) moved uphill.

Gravity and buoyancy are the main driving force. The surface tension was the main constraint on the trajectory of liquid flow, making the liquids move along a very thin layer on the wedge-shaped tracks, that is the liquid flow could move along arbitrary trajectories with the restraint of surface tension. The tilted angle had an influence on the moving velocity of organic liquids, as shown in Fig. 6(b). Take hexane, for example, the velocities increased with an increase of the tilted angle due to the driving force of the component of the buoyancy along the moving direction. Figs. 6(c) and 6(d) show the surface-tension-assisted gravity driven and buoyancy driven underwater SPDT along the spiral track, respectively. Organic liquids could not drop off

in the moving process because of the constraint of surface tension, resulting in the sustained directional transport (Video S7, Supporting Information).

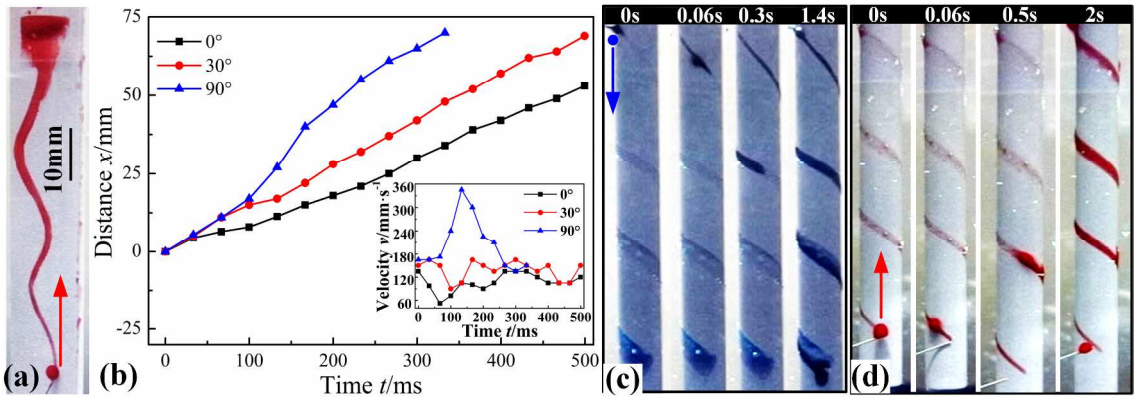

Figure 6. (a) Images of the spontaneous hexane transport with the tilted angle of 90° (*h*=70 mm). (b) Variation in the moving distances of hexane with time at different tilted angles (0°, 30° and 90°) along the track of Fig.6 (a). (c) The spiral downhill process of underwater dichloromethane (*h*=62 mm). (d) The spiral uphill process of underwater hexane (*h*=62 mm).

When gravity and buoyancy were the driving forces, the organic liquids could move farther. For example for hexane, the buoyancy driven hexane could be transported spirally and uphill to a height of 62 mm within 2s [Fig. 6(d)]. While downhill transport with a tilted angle of -8°, the hexane converged at the initial position of the S-shaped track after spreading a length of 32 mm (h≈3mm) [Fig. S5(d)]. Wherein, downhill transport of hexane only showed better effect when the hexane droplets were continuously transported, as the droplets were difficult to drop on the track due to buoyancy.

The equal distribution of underwater liquid droplets was also achieved on the underwater extreme wettability patterns (Fig.7 and Video S8, Supporting Information). A droplet splitter with 4 identical underwater superoleophilic tracks was designed. When the liquid was dropped

on the center of the superoleophilic tracks, the droplets spread rapidly along the four superoleophilic tracks and was transported to the reservoir. When a liquid drop impacts on a solid surface, the droplet would be torn because of that the droplet recoils after the initial spreading stages. However, the droplet recoils only along the superoleophobic background with a great portion of its volume leaving the superoleophilic track at the recoil stage.[29]

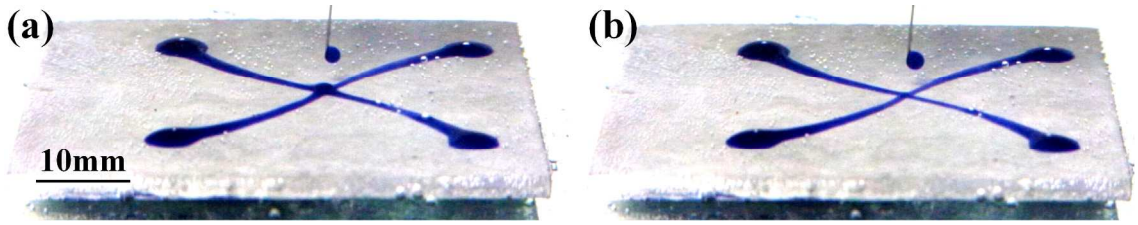

Figure 7. The initial state (a) and the end state (b) of liquid droplets split on the underwater extreme wettability patterns. The droplets were torn under the action of capillary force, and then were transported along the four tracks.

Figure 8 displays the liquid patterning on the underwater extreme wettability patterns. The superhydrophobic region of the underwater extreme wettability patterns produced a brightly mirror-like sheen [Fig. 8(a)]. The liquid droplets were spontaneously and continuously spread along the underwater superoleophilic track, and finally covered the whole pattern [Fig. 8 (c)].

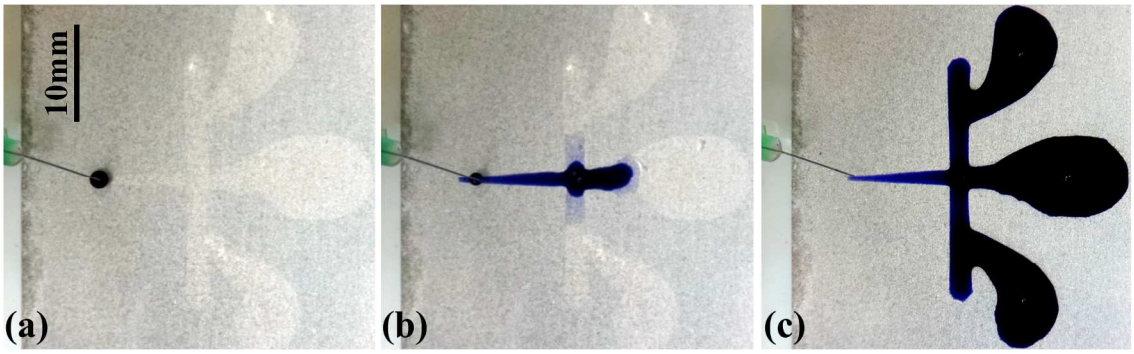

Figure 8. The initial (a), (b) state and the end state (c) of liquid droplets pattern on the underwater extreme wettability patterns. Liquids transport from the starting point of the track and then were full of the pattern.

According to the abovementioned research, we developed a one-way valve for a microfluidic system (Video S9, Supporting Information). The fluid can only flow along the inlet (width: 1mm) to the outlet (width: 2mm), and cannot flow in the opposite direction due to the action of Laplace pressure differences (Video S9, Supporting Information). It is similar to the function of a diode in an electronic, and can maintain good stability even with water sloshing. A magnetic stirrer was used to mix the water. The one-way valve can maintain a good stability against water sloshing when the rotational speed is less than 800 r/min, whereas the dichloromethane would leave the track and the one-way valve did not function at a rotational speed that exceeded 800 r/min.

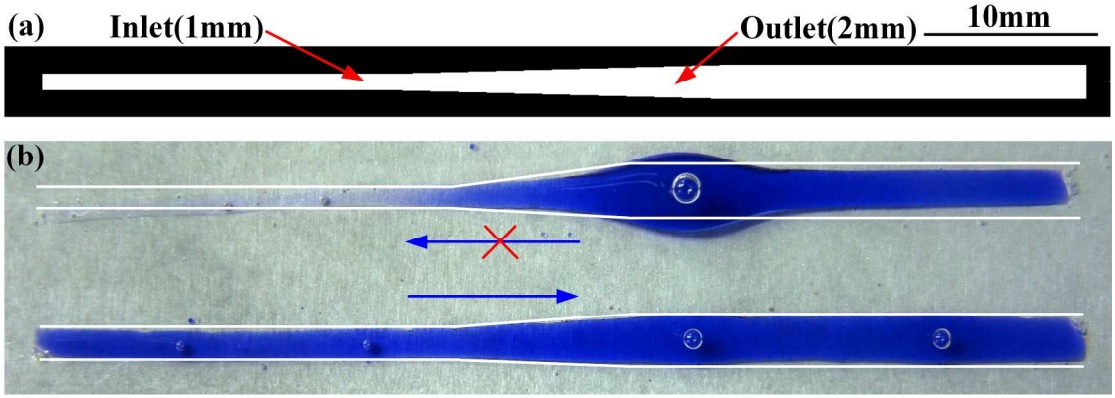

Figure 9. One-way valve of microfluidic system. (a) Schematic diagram and (b) pictures of one-way valve.

3. Conclusion

In summary, we first developed an innovative method to fabricate underwater extreme wettability patterns. $CuCl_2$ etching, stearic acid modification and nitrogen cold plasma jet

treatment with mask were combined to obtain underwater superoleophobic-superoleophilic patterns on Al substrates. Based on this method, we also experimentally and theoretically studied the movement characteristics of the underwater single and continuous organic liquids on the patterns with the wedge-shaped superoleophilic track and superoleophobic background. The wedge angle has a big influence on the velocity and acceleration of the SPHT of organic liquids, and the excellent SPHT of underwater organic liquids was obtained at wedge angle of 3°-5°. The velocities of different organic liquids were proportional to the square root of the ratio of surface tension and kinematic viscosity. The results of the SPTT experiments show that dichloromethane could be uplifted to 11 mm height with a flow rate of 1.14 μL/s when the titled angle was 8°. For the heavier organic liquids driven by gravity and the lighter organic liquids driven by buoyancy, the moving distance and trajectory of SPDT were no longer restricted. We also developed root-like patterns and a one-way valve to enlarge the applicability. This work has application potential in the area of fluid delivery systems, micro detectors and intelligent systems [30-32].

ASSOCIATED CONTENT

Supporting Information

Basic parameters of Organic liquids in the experiments, active particles of atmospheric pressure nitrogen cold plasma, principle of underwater superhydrophobic surface, contact angles of the extreme wettability patterns after nitrogen cold plasma treatment, masking template for the spontaneous transport of hexane with the tilted angles and list of supplementary movies. This material is available free of charge via the Internet at http://pubs.acs.org.

AUTHOR INFORMATION

Corresponding Author

*Jinlong Song, Email: songjinlong@dlut.edu.cn. Phone: (+86)41184708421

Notes

The authors declare no competing finical interest.

ACKNOWLEDGMENT

This work was financially supported by National Natural Science Foundation of China (NSFC, Grant No. 51275072 and No. 51305060) and the Fundamental Research Funds for the Central Universities (DUT15RC(3)066).

REFERENCES

(1) Choi, K.; Ng, A. H.; Fobel, R.; Wheeler, A. R.; Digital Microfluidics. *Annu. Rev. Anal. Chem.* **2012**, *5*, 413-440.

(2) Ghosh, A.; Beaini, S.; Zhang, B. J.; Ganguly, R.; Megaridis, C. M.; Enhancing Dropwise Condensation through Bioinspired Wettability Patterning. *Langmuir* **2014**, *30*, 13103-13115.

(3) Ottesen, E. A.; Hong, J. W.; Quake, S. R.; Leadbetter, J. R.; Microfluidic Digital Pcr Enables Multigene Analysis of Individual Environmental Bacteria. *Science* **2006**, *314*, 1464-1467.

(4) Xia, F.; Jiang, L.; Bio-Inspired, Smart, Multiscale Interfacial Materials. *Adv. Mater.* **2008**, *20*, 2842-2858.

(5) Schutzius, T. M.; Graeber, G.; Elsharkawy, M.; Oreluk, J.; Megaridis, C. M.; Morphing and Vectoring Impacting Droplets by Means of Wettability-Engineered Surfaces. *Sci. Rep.* **2014**, *4*, 7029.

(6) Chaudhury, M. K.; Whitesides, G. M.; How to Make Water Run Uphill. *Science* **1992**, *256*, 1539-1541.

(7) Hernández, S. C.; Bennett, C. J. C.; Junkermeier, C. E.; Tsoi, S. D.; Bezares, F. J.; Stine, R.; Robinson, J. T.; Lock, E. H.; Boris, D. R.; Pate, B. D.; Caldwell, J. D.; Reinecke, T. L.; Sheehan, P. E.; Walton, S. G.; Chemical Gradients On Graphene to Drive Droplet Motion. *Acs Nano* **2013**, *7*, 4746-4755.

(8) Lorenceau, L.; Qur, D.; Drops on a Conical Wire. *J. Fluid Mech.* **1999**, *510*, 29-45.

(9) Ju, J.; Bai, H.; Zheng, Y.; Zhao, T.; Fang, R.; Jiang, L.; A Multi-Structural and Multi-Functional Integrated Fog Collection System in Cactus. *Nat. Commun.* **2012**, *3*, 1247.

(10) Zheng, Y.; Bai, H.; Huang, Z.; Tian, X.; Nie, F.; Zhao, Y.; Zhai, J.; Jiang, L.; Directional Water Collection On Wetted Spider Silk. *Nature* **2010**, *463*, 640-643.

(11) Barman, J.; Swain, D.; Law, B. M.; Seemann, R.; Herminghaus, S.; Khare, K.; Electrowetting Actuated Microfluidic Transport in Surface Grooves with Triangular Cross Section. *Langmuir* **2015**, *31*, 1231-1236.

(12) Khare, K.; Herminghaus, S.; Baret, J.; Law, B. M.; Brinkmann, M.; Seemann, R.; Switching Liquid Morphologies On Linear Grooves. *Langmuir* **2007**, *23*, 12997-13006.

(13) Ghosh, A.; Ganguly, R.; Schutzius, T. M.; Megaridis, C. M.; Wettability Patterning for High-Rate, Pumpless Fluid Transport On Open, Non-Planar Microfluidic Platforms. *Lab Chip* **2014**, *14*, 1538-1550.

(14) Khoo, H. S.; Tseng, F.; Spontaneous High-Speed Transport of Subnanoliter Water Droplet on Gradient Nanotextured Surfaces. *Appl. Phys. Lett.* **2009**, *95*, 063108.

(15) Lv, C.; Chen, C.; Chuang, Y.; Tseng, F.; Yin, Y.; Grey, F.; Zheng, Q.; Substrate Curvature Gradient Drives Rapid Droplet Motion. *Phys. Rev. Lett.* **2014**, *113*, 026101.

(16) Tseng, F.; Lin, K.; Hsu, H.; Chieng, C.; A Surface-Tension-Driven Fluidic Network for Precise Enzyme Batch-Dispensing and Glucose Detection. *Sens. Actuators, A* **2004**, *111*, 107-117.

(17) Yang, I. D.; Chen, Y. F.; Tseng, F. G.; Hsu, H. T.; Chieng, C. C.; Surface Tension Driven and 3-D Vortex Enhanced Rapid Mixing Microchamber. *J. Microelectromech. Syst.* **2006**, *15*, 659-670.

(18) Song, J.; Xu, W.; Liu, X.; Lu, Y.; Wei, Z.; Wu, L.; Ultrafast Fabrication of Rough Structures Required by Superhydrophobic Surfaces On Al Substrates Using an Immersion Method. *Chem. Eng. J.* **2012**, *211-212*, 143-152.

(19) Liu, X.; Chen, F.; Huang, S.; Yang, X.; Lu, Y.; Zhou, W.; Xu, W.; Characteristic and Application Study of Cold Atmospheric-Pressure Nitrogen Plasma Jet. *IEEE Trans. Plasma Sci.* **2015**, *43*, 1959-1968.

(20) Feng, L.; Zhang, H.; Mao, P.; Wang, Y.; Ge, Y.; Superhydrophobic Alumina Surface Based On Stearic Acid Modification. *Appl. Surf. Sci.* **2011**, *257*, 3959-3963.

(21) Lakshmi, R. V.; Basu, B. J.; Fabrication of Superhydrophobic Sol-Gel Composite Films Using Hydrophobically Modified Colloidal Zinc Hydroxide. *J. Colloid Interface Sci.* **2009**, *339*, 454-460.

(22) Saleema, N.; Farzaneh, M.; Thermal Effect on Superhydrophobic Performance of Stearic Acid Modified Zno Nanotowers. *Appl. Surf. Sci.* **2008**, *254*, 2690-2695.

(23) Chen, F.; Xu, W.; Lu, Y.; Song, J.; Huang, S.; Wang, L.; Parkin, I. P.; Liu, X.; Hydrophilic Patterning of Superhydrophobic Surfaces by Atmospheric-Pressure Plasma Jet. *Micro Nano Lett.* **2015**, *10*, 105-108.

(24) Cheng, Q.; Li, M.; Zheng, Y.; Su, B.; Wang, S.; Jiang, L.; Janus Interface Materials: Superhydrophobic Air/Solid Interface and Superoleophobic Water/Solid Interface Inspired by a Lotus Leaf. *Soft Matter* **2011**, *7*, 5948.

(25) Brinkmann, M.; Lipowsky, R.; Wetting Morphologies on Substrates with Striped Surface Domains. *J. Appl. Phys.* **2002**, *92*, 4296.

(26) Darhuber, A. A.; Troian, S. M.; Reisner, W. W.; Dynamics of Capillary Spreading Along Hydrophilic Microstripes. *Phys. Rev. E.* **2001**, *64*, 031603.

(27) Schutzius, T. M.; Elsharkawy, M.; Tiwari, M. K.; Megaridis, C. M.; Surface Tension Confined (Stc) Tracks for Capillary-Driven Transport of Low Surface Tension Liquids. *Lab Chip* **2012**, *12*, 5237-42.

(28) Washburn, E. W.; The Dynamics of Capillary Flow. *Phys. Rev.* **1921**, *17*, 273.

(29) Lee, M.; Chang, Y. S.; Kim, H.; Drop Impact on Microwetting Patterned Surfaces. *Phys. Fluids* **2010**, *22*, 072101.

(30) Liu, K.; Wu, R.; Chuang, Y.; Khoo, H. S.; Huang, S.; Tseng, F.; Microfluidic Systems for Biosensing. *Sens.* **2010**, *10*, 6623-6661.

(31) Tian, Y.; Su, B.; Jiang, L.; Interfacial Material System Exhibiting Superwettability. *Adv. Mater.* **2014**, *26*, 6872-6897.

(32) Xia, F.; Jiang, L.; Bio-Inspired, Smart, Multiscale Interfacial Materials. *Adv. Mater.* **2008**, *20*, 2842-2858.

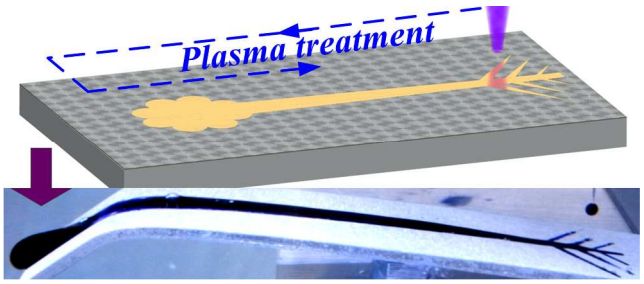

Table of Contents